

Stiffness profile spectral composition & geometry deterioration of railway tracks

Lu, Tao; Chen, Rong; Wang, Ping; Wu, Junwei; Steenbergen, Michaël

DOI

[10.1016/j.engstruct.2023.116966](https://doi.org/10.1016/j.engstruct.2023.116966)

Publication date

2023

Document Version

Final published version

Published in

Engineering Structures

Citation (APA)

Lu, T., Chen, R., Wang, P., Wu, J., & Steenbergen, M. (2023). Stiffness profile spectral composition & geometry deterioration of railway tracks. *Engineering Structures*, 296, Article 116966. <https://doi.org/10.1016/j.engstruct.2023.116966>

Important note

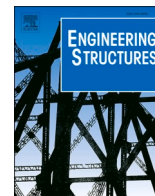
To cite this publication, please use the final published version (if applicable). Please check the document version above.

Copyright

Other than for strictly personal use, it is not permitted to download, forward or distribute the text or part of it, without the consent of the author(s) and/or copyright holder(s), unless the work is under an open content license such as Creative Commons.

Takedown policy

Please contact us and provide details if you believe this document breaches copyrights. We will remove access to the work immediately and investigate your claim.



Stiffness profile spectral composition & geometry deterioration of railway tracks

Tao Lu^{a,b}, Rong Chen^{a,c}, Ping Wang^{a,c}, Junwei Wu^{a,c}, Michaël Steenbergen^{d,*}

^a MOE Key Laboratory of High-Speed Railway Engineering, Southwest Jiaotong University, 610031 Chengdu, China

^b SWJTU-Leeds Joint School, Southwest Jiaotong University, 611756 Chengdu, China

^c School of Civil Engineering, Southwest Jiaotong University, 610031 Chengdu, China

^d Section of Mechanics and Physics of Structures, Faculty of Civil Engineering and Geosciences, Delft University of Technology, Stevinweg 1, 2628 CN Delft, The Netherlands

ARTICLE INFO

Keywords:

Track degradation
Track stiffness
Energy dissipation
Track stiffness variation
Track stiffness profile

ABSTRACT

This work addresses the contribution of the wavelength composition of the spectrum of the rail support stiffness profile to the expected long-term settlement. To that aim, purely harmonic stiffness variations of different wavelength are studied. The frequency-domain model with a double periodicity level previously developed by the first and last authors is adopted to embed the stiffness profile in one of the periodicity layers. Additional resonance velocities at which the resonance frequency of the track system coincides with the support-passing frequency or its multiples are found. The susceptibility to degradation is assessed both by quantifying the mechanical energy dissipated in the substructure under a moving train axle within one wavelength of the support stiffness variation, and the work performed by the wheel-rail contact force. It is shown that shorter wavelengths and larger standard deviations of varying ballast/subgrade stiffness result in an increasing energy dissipation in the substructure, and increase the work performed by the wheel-rail contact force, therefore leading to a reduced lifetime of the track. The energetic quantities increase for lower mean values of the stiffness profile, confirming the proneness of tracks on soft soils to degradation. The influence of varying stiffness vanishes for wavelengths of approximately 16 times the sleeper span, which is equivalent to a track length of about 10 m. High railpad stiffness values result in increased energy dissipation but the influence is limited. In general, an increasing train velocity amplifies the rate of track degradation, with no stabilizing trend in the high-speed regime (300 km/h).

1. Introduction

Degradation of track geometry under train loading, with the need for tamping and correction of the track geometry, is the other side of the coin that belongs to the historical concept of a ballasted train track, where the geometry of the rail remains adjustable at any moment during the structural lifecycle. In the scarce early scientific literature on the domain, mainly empirical methods were discussed to predict the process of track geometry degradation [1–5]. These methods were often site-specific and not generally applicable. In recent years, data-driven predictive models [5–7] have been proposed to explore the degradation of track geometry as a function of the traffic load and track parameters, whereas experimental work was published to elucidate more explicitly the relationship between track stiffness and track geometry [3,8,9]. Another category of studies dealt with the relationship between track

geometry, variation in track properties and train-induced vibration, both numerically and analytically, such as reported in [10–26]. Most of these contributions considered randomness of support stiffness and its influence on vehicle and/or track vibration [10–16,18,19,21,23,24]. Local variation of support stiffness was considered in the form of transition zones in [20,27,28] and hanging sleepers in [22,26]. In [25], a harmonically varying foundation stiffness was considered, showing its effect on the dynamic response of the railway track. The study adopted a Winkler type of foundation, ignoring the discrete nature of the supports.

Though the role of the subsoil with respect to track degradation is well-known and documented in the literature [1,29–31], in the sense that tracks on poor soil conditions need relatively intense maintenance, the effect of non-uniformity in the profile of the support stiffness along the track on this process is much less understood and explored. This is in particular true in the context of a fundamental understanding and

* Corresponding author.

E-mail address: m.j.m.m.steenbergen@tudelft.nl (M. Steenbergen).

<https://doi.org/10.1016/j.engstruct.2023.116966>

Received 15 June 2023; Received in revised form 12 September 2023; Accepted 24 September 2023

Available online 30 September 2023

0141-0296/© 2023 The Authors. Published by Elsevier Ltd. This is an open access article under the CC BY license (<http://creativecommons.org/licenses/by/4.0/>).

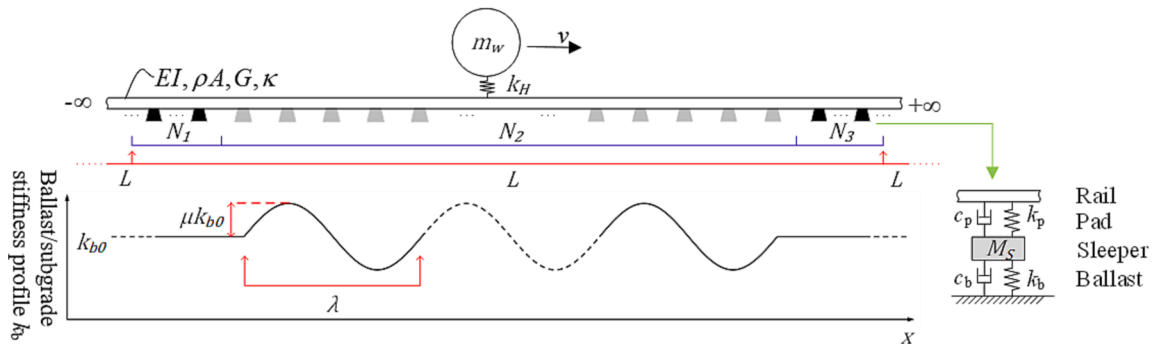


Fig. 1. Schematic model overview of the model for non-uniform track.

conceptual framework of track geometry degradation.

Railway tracks are loaded, in the vertical plane, by a history of moving axle loads with a static and a dynamic component. The static component is directly governed by the mass of the car body itself and its loading; it is therefore the essence of transport and cannot be avoided. On the contrary, the dynamic axle load does not belong to this essence, but is a kind of by-product generated by different sources as a consequence of the moving character of the load. Most importantly, the primary sources are: wheel out of roundness of the rolling stock, and on the side of the infrastructure, the track geometry (deviation from the straight line) and the stiffness profile (variation in support stiffness along the rail) [9,16,18,19,21–25]. The presence of a dynamic axle load has negative influences on the rail transport system as a whole: it increases the energy consumption of the locomotive, and the mechanical energy it generates in the wheel-rail contact interface leads to the emission of environmental vibration (by means of wave propagation or radiation of energy) [18,32,33] and the degradation of the track geometry (by means of dissipation of energy along the radiation path) [22,23].

Degradation can, in principle and as far as it is driven by train operation, be related to both the static and the dynamic axle load. The track system response to a loading process of a moving, purely static load consists, for subcritical train speeds, of a deflection field which moves in space while remaining constant in time. The nature of this response depends on the material properties concerned, but every response that is not purely elastic will lead to incremental degradation: viscous behavior leads to dissipation of mechanical energy into heat, for example by friction of ballast particles leading to wear which will affect the constitutive behavior of the granular matrix, while any form of plasticity implies irreversible displacement and strain accumulation, for example leading to rearrangement of ballast particles or differential settlement. It is however a property of this form a degradation that it is, like the response field itself, constant in space. In other terms: it leads to uniform settlement. Moreover, like the response field itself, it is confined in space, having an influence radius governed by the magnitude (and speed) of the axle load. It has therefore no implications in a moving reference frame such as the one moving with the wheel-rail contact position. It must be added here that a track system with a purely static moving axle load can only exist if the primary sources of a dynamic axle load are absent, i.e. for a perfectly straight and perfectly uniform track. The response to the dynamic axle load consists of a wave field that is emitted from the moving contact position and radiated in space, including both the surface coordinates but also the depth coordinate. On the radiation path, the energy of the wave field decays due to dissipation, again by viscosity and other types of material damping. Since the dynamic axle load is by definition not constant in space, also the energy that is dissipated within and underneath the track body is not constant along the system, which has as a consequence differential settlement. Contrary to uniform settlement, this form of settlement does affect the track geometry and will further amplify the dynamic axle load itself.

This argument highlights the importance of the dynamic axle load in the understanding, analysis and mitigation of track degradation.

Previous work in the domain [9,22,23,34] has highlighted the role of the track stiffness and its spatial variation in generating a dynamic axle load and promoting track degradation. The principal aim of the present work is to further study and quantify the role of the support stiffness profile and its specific appearance forms in degradation of the track under train loading. Since arbitrary profiles have a spectrum and can be decomposed and expressed in terms of harmonics of different wavelengths, this work focusses on harmonic ballast/subgrade stiffness profiles in space. It is well-known from practice that deterioration starts locally and expands globally, implying that the track irregularity spectrum develops over time not only in magnitude but also in wavelength content. This study addresses the novel question whether the presence of specific wavelengths in the stiffness profile (or spectrum) of a given track trigger the degradation process – and should therefore receive particular attention in terms of monitoring and maintenance. The theoretical approach taken is the same as in previous work and based on conservation of energy: it is assumed that both the work done by the wheel-rail contact force over a certain track length and the energy dissipated within the structure are indicators for track degradation and have predictive value. Even though the exact amount of energy is strongly dependent on modeling choices and descriptions (such as damping), the intensity of its variation in space is much less dependent on these choices. The strength of the adopted approach is therefore that it allows for indicators to be established for the rate of degradation that will occur in the system, even when, in order to quantify the degradation itself over time, an iterative approach would be needed [19,21,28,30,35].

2. Theoretical basis

2.1. Model description

As shown in Fig. 1, the railway track model represents a half track and consists of a rail (modelled by the Timoshenko beam) and equidistant, discrete supports. At each support, a railpad with stiffness k_p and viscosity c_p is in between the rail and the sleeper with mass M_s . Under the sleeper, the ballast/subgrade is characterized by its stiffness k_b and damping coefficient c_b . A moving mass M_w (representing the unsprung wheel mass) at a steady velocity v is coupled with the rail by linearized Herz contact spring with stiffness k_H . As shown in [22,23], the non-uniform supports (in our case a range of supports with harmonically varying ballast stiffness) are embedded in the section N_2 , jointed by identical sections N_1 and N_3 at both sides of N_2 section. The section $N_1 + N_2 + N_3$ assembles a new period and repeats itself in space to form a periodical structure. The number of sections needed for a converged result is designated as NOS. For more details of the model employed and the mathematical derivation, one is referred to [22,23].

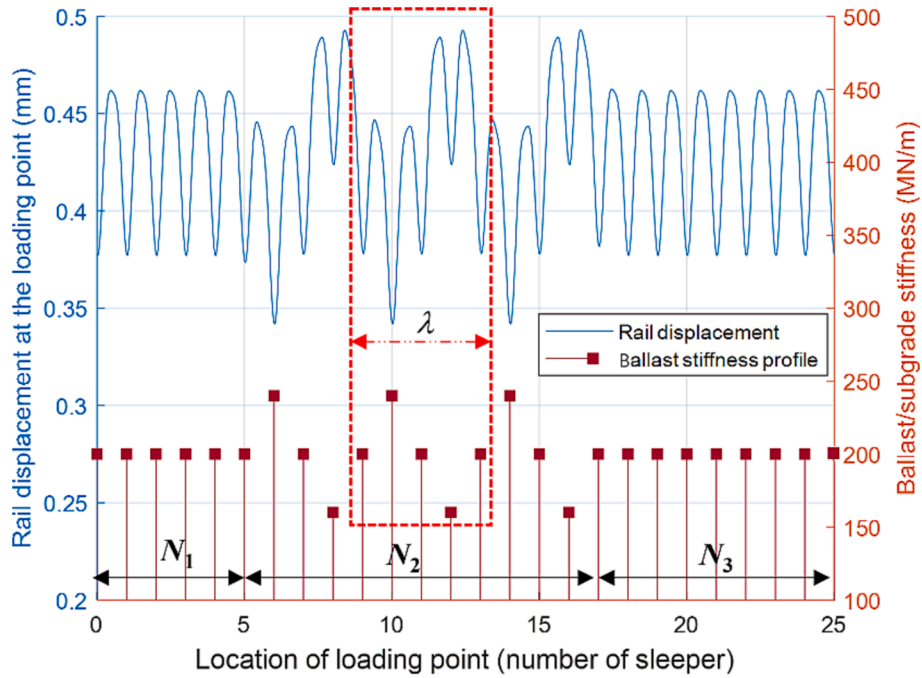


Fig. 2. Convergence check of the number of wavelengths in section N_2 .

2.2. Embedding harmonically varying ballast/subgrade stiffness in the model

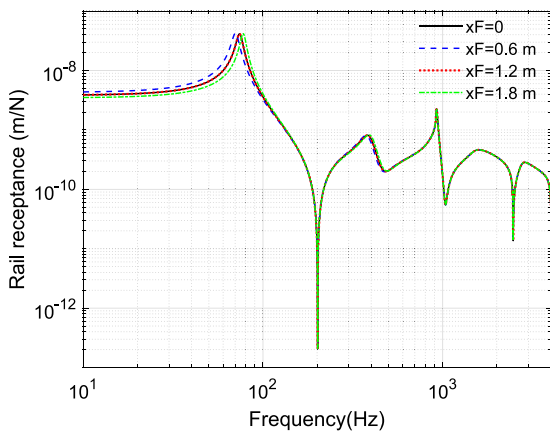
In the non-uniform region shown in Fig. 1, the ballast/subgrade stiffness profile is assumed to have the following expression:

$$k_b(x) = k_{b0} \left[1 + \mu \cos\left(\frac{2\pi x}{\lambda}\right) \right], \quad (1)$$

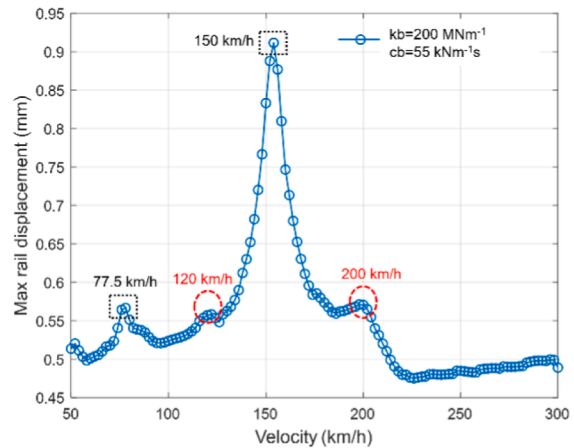
in which k_{b0} is the stiffness of ballast/subgrade in the uniform sections, λ is the wavelength of the varying stiffness and μ is a parameter representing the level of amplitude variation of the support stiffness from its mean value. μ can be considered as the standard deviation of the ballast/subgrade stiffness in the non-uniform section as well. The coordinate x takes the values which correspond to positions of sleepers. In this section, the spatial wavelength of stiffness variation is chosen to be in the range $4l_s \leq \lambda \leq 16l_s \approx 10$ m. In this range, the minimum wavelength is described by the strict minimum of 5 support positions, whereas the maximum is more arbitrarily chosen at the value of 10 m, where it is

taken into account that the effect of the wavelength is expected to vanish for large wavelengths (this choice will be justified in Section 4.1). To make sure that the peak values of stiffness described by Eq. (1) are assigned at sleepers, the representative wavelength λ is chosen to be $4l_s, 8l_s, 12l_s, 16l_s$ in our simulations hereafter.

To eliminate non-physical effects due to transition from uniform support to non-uniform support conditions, several wavelengths should be considered in the non-uniform section N_2 . The region of interest is somehow in the middle part of section N_2 in which the response should be steady and the effects of transition from N_1 to N_2 and from N_2 to N_3 should be eliminated based on the choice of number of wavelengths for the harmonic variation of stiffness embedded in section N_2 . In Fig. 2, such a check is presented. The ballast/subgrade stiffness profile is plotted in the lower part of the figure with the discrete stiffness values represented by the y-axis at the right. The rail displacement under the loading point is illustrated in the upper part of the figure and its magnitudes are shown on the y-axis at the left. The horizontal axis shows the position of loading points represented by the number of sleepers



(a) Rail receptance (xF denotes the location of the oscillator)



(b) Resonance speeds

Fig. 3. Resonance velocity induced by spatial periodicity of the track for a moving mass case.

Table 1

Values of the system parameters of the model used in the parametric study [22]:

Parameters	Values
Rail bending stiffness (EI), MNm ²	4.25 (54E1 profile)
Rail mass per length (ρA), kgm ⁻¹	54.4 (54E1 profile)
Sleeper mass (M_s), kg	142.5
Distance between sleepers (l_s), m	0.6
Railpad stiffness (k_p), MNm ⁻¹	1000*
Railpad damping (c_p), kNm ⁻¹ s	30-
Ballast stiffness (k_b), MNm ⁻¹	50
Ballast damping (c_b), kNm ⁻¹ s	55
Wheel unsprung mass (M_w), kg	900

* The pad stiffness of 1000 MN/m corresponds to the Corkelast pad used for typical Dutch track.

(position of sleepers). In section N_2 , three full wavelengths of stiffness variation are included. It can be seen that in this case, the response in the area of the central wavelength (the area in the dashed rectangle) is not affected by the transitions between N_1 - N_2 and N_2 - N_3 . Therefore, the analysis can be done based on results in this area. Note that the needed number of spatial periods (wavelengths of Eq. (1)) varies for different velocities and system parameters and therefore should be justified case to case.

3. Resonance velocities in periodically varying track traversed by a mass

In contrast to the moving load situation, the moving mass introduces an interaction force which can be expressed by Fourier series due to the periodicity of the wheel-rail system as [22]:

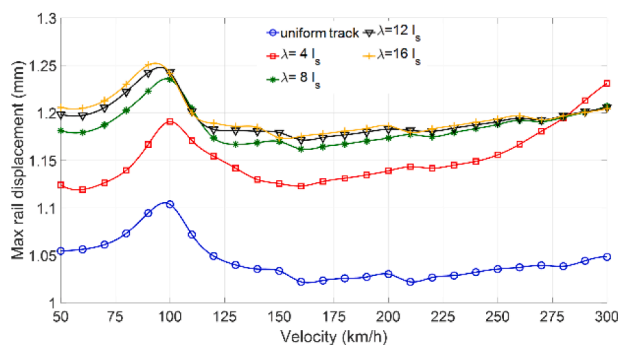
$$F_c(t) = \sum_{m=-\infty}^{+\infty} \bar{F}_m e^{jm \left(\frac{2\pi}{L} \right) t} \quad (2)$$

in which L is the length of the spatial period $N_1 + N_2 + N_3$ section. The frequency components of the Fourier series equal the spatial period-passing frequency and its multiples [22]. In this sense, one would expect resonance of the wheel-rail system to occur at the velocity which in combination with a certain track periodicity gives a passing frequency - or its multiples - coinciding with one of the peaks of the rail receptance. When a harmonically varying support stiffness is included, a new spatial periodicity is introduced. Maximum responses of the system are expected when:

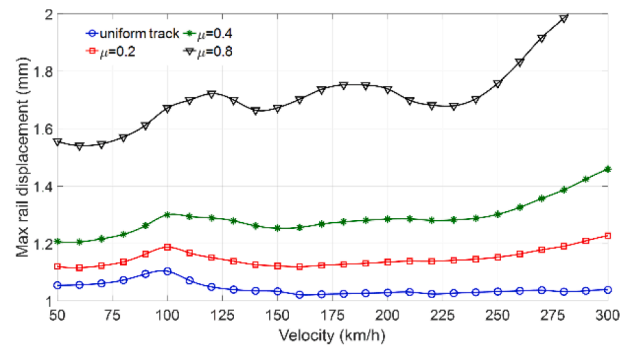
$$f_p = p \frac{v}{l_s}, \quad p = 1, 2, 3, 4, \dots \quad (3)$$

for the sleeper-passing frequency and

$$f_p = n \frac{v}{\lambda}, \quad n = 1, 2, 3, 4, \dots \quad (4)$$



(a) $\mu = 0.2$



(b) $\lambda = 4l_s$

Fig. 4. Rail maximum displacement versus velocity (nominal values of parameters in Table 1).

for the harmonic support-passing frequency. In Eqs. (3–4), f_p is the peak frequency of the rail receptance which can be calculated according to [22]. In Fig. 3, the above argument is validated by examining the rail response versus the velocity of the moving mass. The ballast/subgrade stiffness is chosen to be 200 MNm⁻¹ and a constant damping value 55 kNm⁻¹s is adopted for the purpose to better visualise the resonance velocities. $\lambda = 4l_s$ and $\mu = 0.2$ are used to characterize the harmonically varying stiffness profile. Other parameters are all according to the nominal values listed in Table 1. In Fig. 3 (a), the receptance of the rail with harmonically varying ballast stiffness is plotted for different locations of the harmonic point load/wheel position. It can be seen that the first resonance frequency varies along with this position. At higher frequencies, positions of the harmonic point load do not influence the rail receptance. The first resonance frequency of the rail displacement varies within a bandwidth but is about 72 Hz on average for the selected parameters. In Fig. 3 (b), resonance velocities are shown. The peaks at $v = 150$ km/h and 77.5 km/h correspond to Eq. (3) when $p = 1$ and 2, respectively. The peaks at $v = 200$ km/h and 120 km/h are related to Eq. (4) for the case of $n = 3$ and 5, respectively. It is thus concluded that the introduction of harmonically varying support stiffness causes extra resonance speeds of the moving train. Note that not all theoretically predicted peaks by Eqs. (3–4) will be visible in the rail displacement-velocity plots since the magnitudes of responses at those speeds depend on the system parameters, especially the damping values. This holds for other system parameters, especially when the ballast/subgrade is relatively soft with a relatively high damping.

4. Degradation in railway tracks with harmonically varying support stiffness

In this section, the influence of the wavelength itself and the standard deviation of the varying stiffness on the energy dissipation, as an indicator for track degradation, will be considered. Since the ballast/subgrade stiffness and the railpad stiffness are design parameters which can be adjusted in practice, their influence on track degradation will also be explored.

4.1. Spatial resolution of stiffness variation

From reference [21], the standard deviation of ballast/subgrade stiffness divided by the mean value of the dataset equals 0.17 for Site A and 0.13 for Site B. In previous work by a subset of the authors [23], this ratio is 0.30, 0.15 and 0.24, respectively for the three datasets collected from literature. In this section, three values of μ are assumed, namely 0.2, 0.4 and 0.8 to represent different levels of variability of the ballast/subgrade stiffness. The first two values are close to ones used in the literature [21,23] whereas the last one is selected to be large enough to represent also extreme cases of spatial variation of support stiffness.

In Fig. 4, the maximum displacement of the rail under the wheel

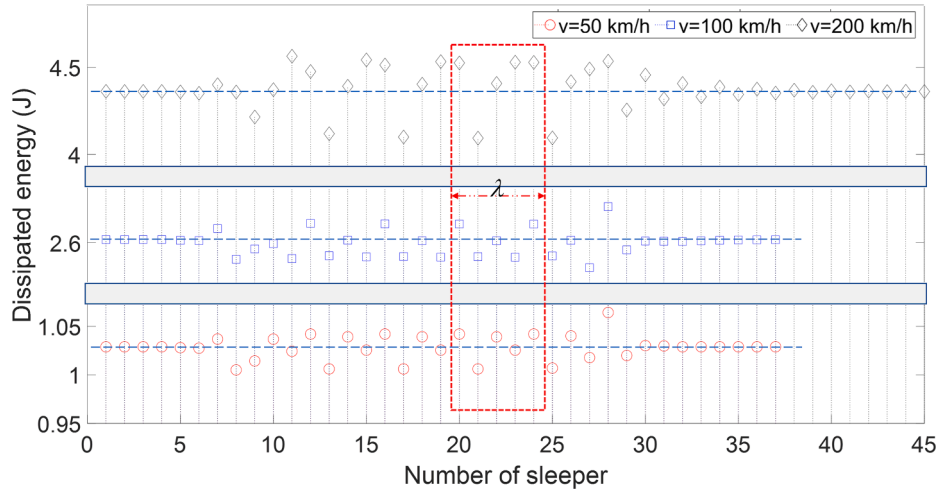


Fig. 5. Dissipated energy in supports for various velocities ($\mu = 0.2$ and $\lambda = 4l_s$, nominal values for other parameters in Table 1).

loading position is plotted against the velocity of the train. In this figure, the graph for the “uniform track” case refers to one single sleeper bay, which is the elementary periodicity of the system. Nominal values from Table 1 are chosen which result in 45 Hz of the first resonance peak of the rail receptance. Therefore, the major resonance speed which corresponds to $p = 1$ in Eq. (3) approximately equals 97 km/h. The uniformly supported track ($\mu = 0$) is also plotted as a reference. In Fig. 4(a), μ is fixed to 0.2 and the wavelength of the ballast stiffness varies from $4l_s$ to $16l_s$ (or about 10 m). It can be found for the adopted parameters that the maximum displacement of the rail increases with this wavelength. Meanwhile, the velocity corresponding to the major peak value of the rail displacement shifts to a lower speed which is in agreement with [25]. With increasing wavelength, the effect of harmonically varying stiffness tends to converge, especially at speeds larger than 200 km/h. In Fig. 4(b), λ is fixed to $4l_s$ whereas μ varies from 0.2 to 0.8. It can be concluded that the rail displacement grows with increasing variability of ballast/subgrade stiffness. Also, more velocities with peak responses appear as the variability of the ballast stiffness intensifies.

In Fig. 5, the energy dissipation in the supports is shown for various velocities. The energy dissipation in the i th support is obtained by [22]:

$$E_{\text{diss},i} = \int_{-\infty}^{+\infty} f_{d,i}(t)v_{s,i}(t) dt = \int_{-\infty}^{+\infty} c_{b,i}v_{s,i}(t)^2 dt, \quad (5)$$

where $v_{s,i}(t)$ is the velocity response of the i th sleeper in the time domain and $c_{b,i}$ is the viscous damping below the i th sleeper. In section N_2 , several wavelengths are embedded to achieve a steady state response in one wavelength as indicated in the red box. It can be observed that the lengths of the uniform sections N_1 and N_3 are chosen such that convergent results are obtained compared to corresponding uniform tracks (indicated by the horizontal, dashed lines). It can be concluded that the dissipated energy increases for higher velocities of the moving mass. On the other hand, higher velocities also result in larger oscillations of the dissipated energy in space.

In analogy to the approach adopted in [22,23], two statistical quantities are adopted to describe the expected degradation in terms of energy dissipation over one wavelength of the non-uniform zone in Fig. 6:

- The root mean square (denoted as RMS) of energy dissipation in one wavelength:

$$E_{\text{diss,rms}} = \sqrt{\frac{1}{N} \sum_{i=1}^N E_{\text{diss},i}^2} \quad (6)$$

in which N is the number of sleepers in one wavelength of varying

stiffness, e.g. number of sleepers in the dashed rectangle in Fig. 2.

- The maximum spatial gradient of dissipated energy in one wavelength:

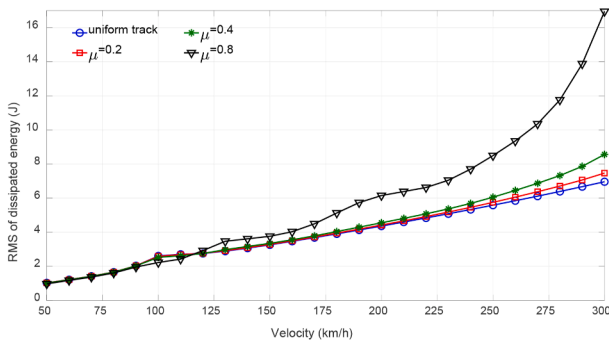
$$\text{MDD} = \max|\epsilon| \quad (7)$$

in which the vector ϵ is assembled by $\epsilon_i = E_{\text{diss},i+1} - E_{\text{diss},i}$ where $i = 1, 2, \dots, N$.

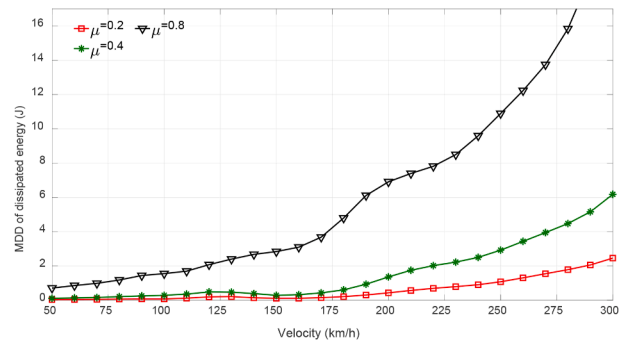
In addition, the work done by the wheel-rail contact force is also depicted both for its RMS and maximum values, for one single wavelength of stiffness variation. From Fig. 6, it is clear that generally speaking the energy dissipation increases with increasing train velocities, where the effect of both the intensity of variation and its wavelength are much more pronounced for MDD as compared to RMS, indicating localized effects on settlement. RMS of dissipated energy increases with larger variation of support stiffness. In particular, RMS is rather insensitive to the wavelength of stiffness variation (Fig. 6(e)). MDD of dissipated energy is very sensitive to variation of both the magnitude of stiffness variation and its wavelength, with increasing differential settlement expected for increasing stiffness variation and smaller wavelengths. The dependence of the maximum work done by the wheel-rail contact force upon velocity is similar to that of the maximum displacement of the rail, as is clear from a comparison of Fig. 4 with Fig. 6(d,h). The global trend of RMS of the work performed by the contact force is similar to that of RMS of dissipated energy, although the influence of stiffness variation and its wavelength is much more pronounced on the work. It is also noticed that in Fig. 4(a) and Fig. 6(e-h), the maximum displacements, the dissipated energy and the work done by contact force start to converge when the wavelength reaches approximately $16l_s$. This confirms the expectation that the effect of stiffness variation - for the elementary case of one single moving axle without coupling or interaction in a bogie or car body - vanishes when its wavelength is in the order of magnitude of 10 m.

In Fig. 7, the standard deviation (STD) of dissipated energy in the supports is illustrated. Compared to Fig. 6(b) and (f), it can be concluded that the STDs have similar trends as MDDs of the dissipated energy. This can be expected since both quantities are similar in nature, both of them being an indicator for the width of the statistical distribution of the dataset or the occurrence of local extremes, independent from the average.

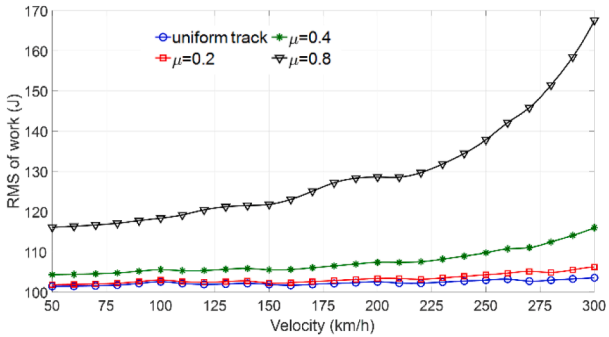
The energy indicators for typical train velocities are highlighted in Fig. 8 for four different wavelengths of the supporting stiffness. It can be seen once again that RMS of dissipated energy is rather insensitive to wavelength, whereas the MDD trend clearly stipulates the role of shorter wavelengths of varying stiffness as local initiators of track degradation,



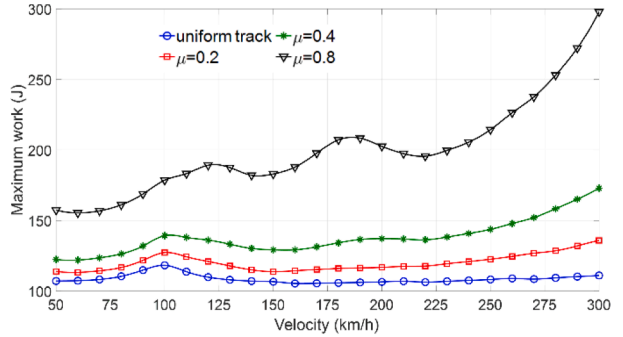
(a) $\lambda = 4l_s$, RMS of dissipated energy in a wavelength



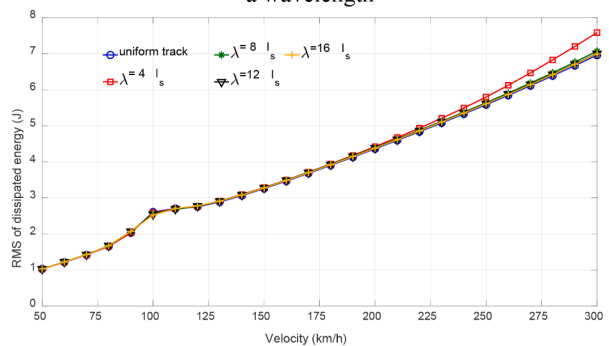
(b) $\lambda = 4l_s$, MDD of dissipated energy in a wavelength



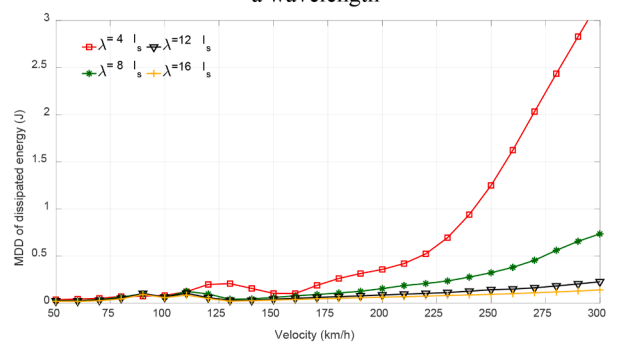
(c) $\lambda = 4l_s$, RMS of the work done by the contact force over a wavelength



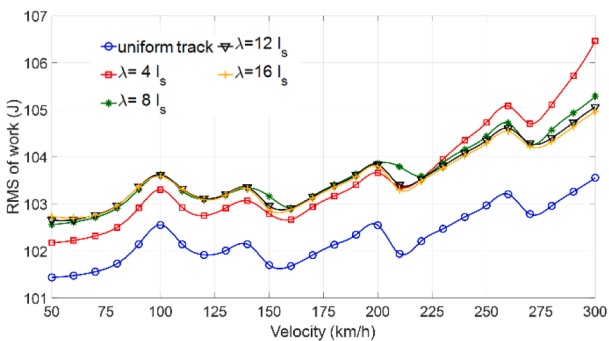
(d) $\lambda = 4l_s$, maximum work done by the contact force within a wavelength



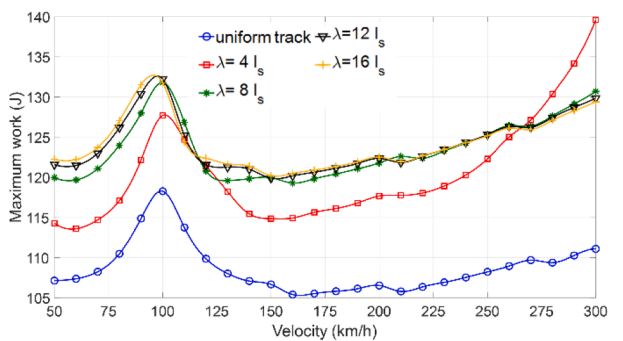
(e) $\mu = 0.2$, RMS of dissipated energy in a wavelength



(f) $\mu = 0.2$, MDD of dissipated energy in a wavelength



(g) $\mu = 0.2$, RMS of the work done by the contact force over a wavelength



(h) $\mu = 0.2$, maximum work done by the contact force within a wavelength

Fig. 6. The dissipated energy and the work done by the contact force.

specifically for increasing train velocities.

In reality, the distribution of ballast stiffness along the railway track consists of multiple harmonics of different wavelength. Therefore, in Fig. 9, three combinations of stiffness profiles of $\lambda = 4l_s, 8l_s, 16l_s$ are studied, all of them with the same mean value and standard deviation;

only the phases differ. The three combined stiffness distributions are shown in Fig. 9(a). Since $\lambda = 4l_s, 8l_s, 16l_s$ have common multiples, their superposition yields periodical distributions in space as well. Therefore, in Fig. 9(b-d) the statistical indicators of dissipated energy are shown in the common period in space as shown in Fig. 9(a). It can be concluded

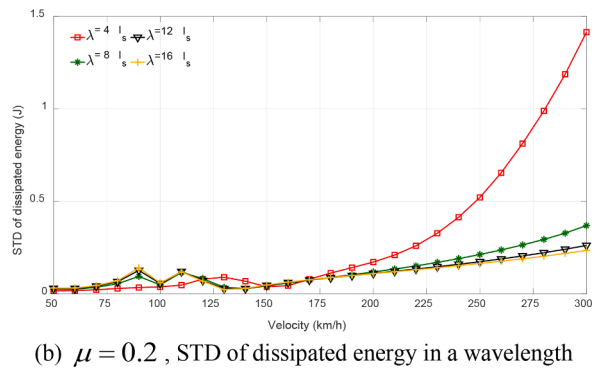
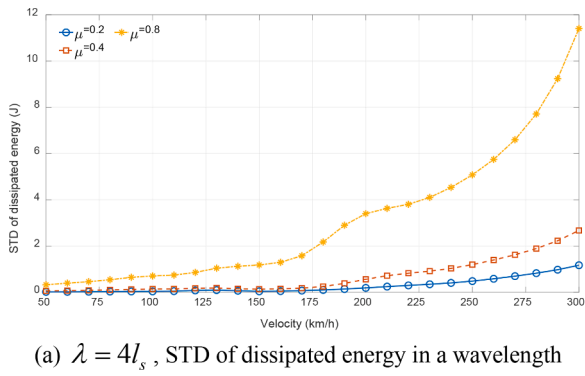


Fig. 7. The standard derivation (STD) of dissipated energy.

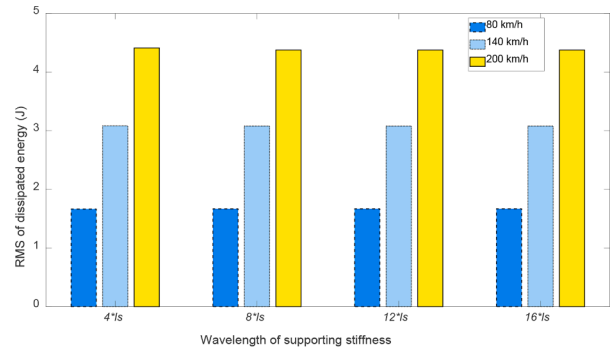
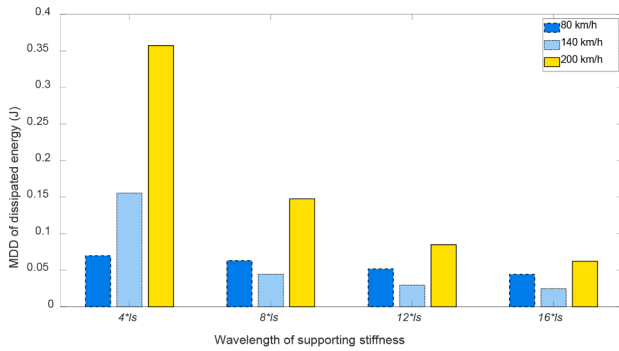


Fig. 8. Energy indicators for typical train velocities (freight and passengers).

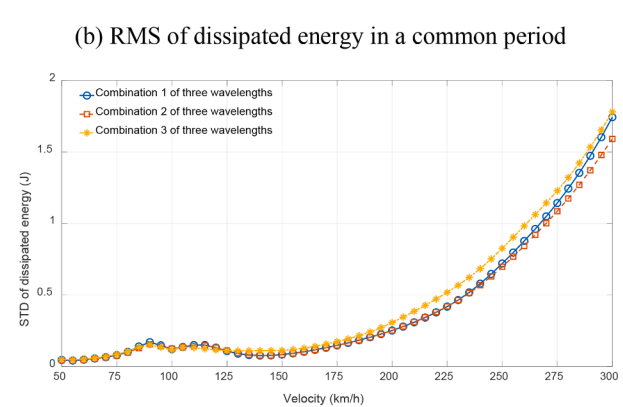
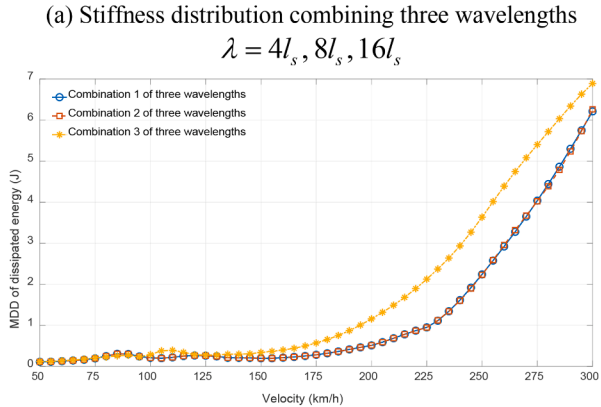
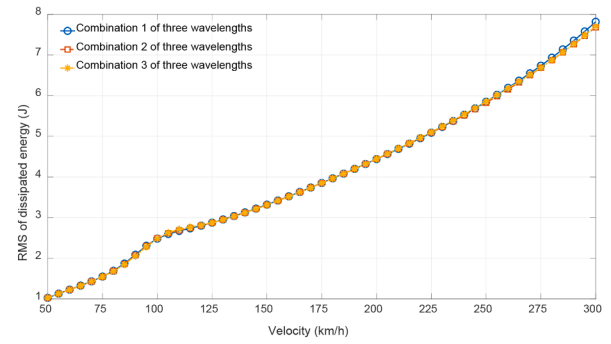
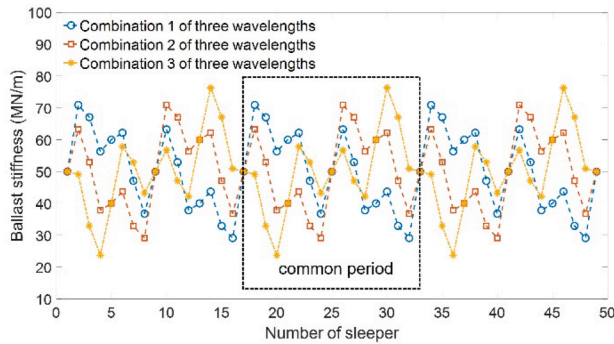


Fig. 9. Energy dissipation in three non-uniform sections with three wavelengths combined (in each non-uniform section, the same mean value and standard deviation of ballast stiffness are used).

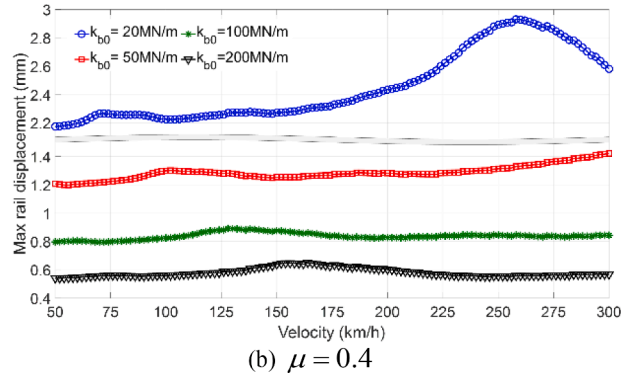
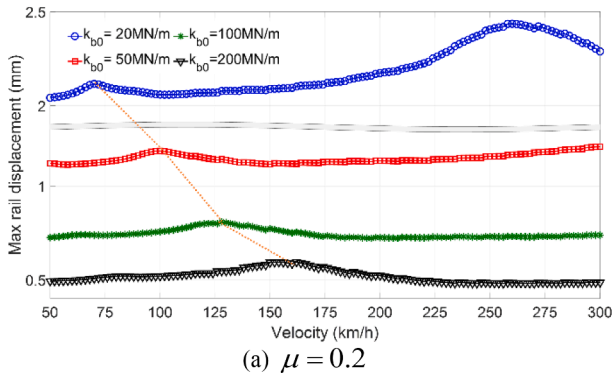
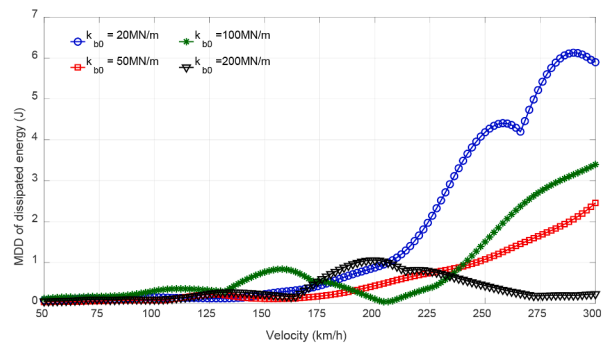
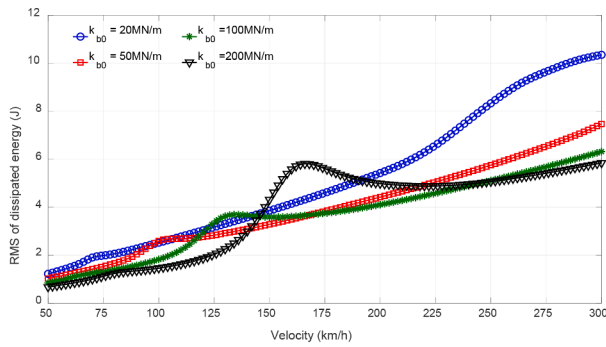
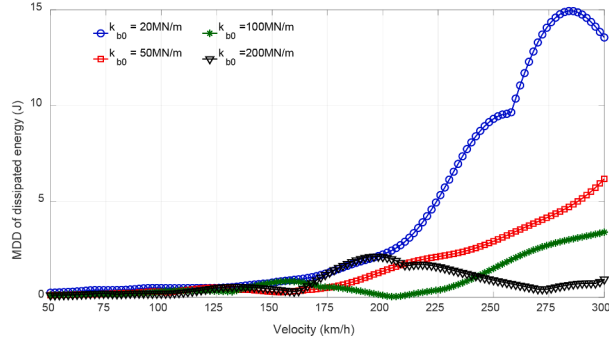
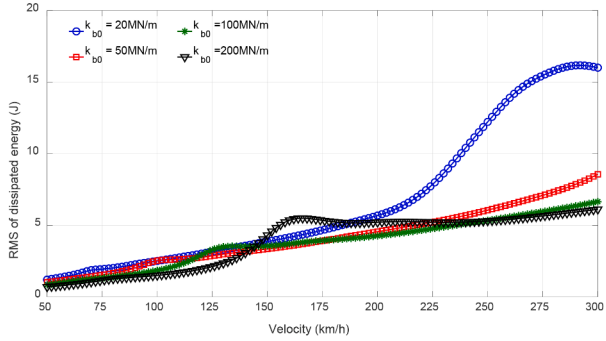


Fig. 10. Rail maximum displacement versus velocity ($\lambda = 4l_s$), different ballast/subgrade stiffness.



(a) $\mu = 0.2$, RMS of dissipated energy in a wavelength

(b) $\mu = 0.2$, MDD of dissipated energy in a wavelength



(c) $\mu = 0.4$, RMS of dissipated energy in a wavelength

(d) $\mu = 0.4$, MDD of dissipated energy in a wavelength

Fig. 11. RMS and MDD of dissipated energy ($\lambda = 4l_s$), different ballast stiffness.

that the RMS of energy dissipation is nearly identical, and therefore rather independent from the phases of the harmonics. The MDD and STD are similar at low velocities and show larger discrepancy at high velocities, for which the phase configuration becomes relevant. The findings are in line with previous work in [22,23].

4.2. Influence of ballast/subgrade stiffness

In this section, the influence of ballast/subgrade stiffness on the energy dissipation (and therefore, expected degradation) is analyzed. The wavelength of spatially varying stiffness is fixed at $\lambda = 4l_s$ whereas the standard deviation μ varies, keeping in mind that the result of the previous section with respect to the effect of the wavelength itself. A constant ratio between the ballast damping and the ballast stiffness is kept for all the ballast/subgrade stiffness values (which is $r = 55e3/50e6$ according to Table 1).

In Fig. 10(a), one can see that the first resonance velocity shifts with increasing ballast/subgrade stiffness as expected. For soft ballast, there

is another, much wider peak at velocities beyond 250 km/h. The dotted line in the Figure shows the increase of the first resonance velocity from about 70 km/h to 160 km/h as the mean value of the ballast stiffness changes from 20 MN/m to 200 MN/m. As the deviation from the mean value increases, the resonance velocities remain nearly unaltered whereas the response magnitudes increase as shown in Fig. 10(b).

As to the dissipated energy in the supports shown in Fig. 11, the RMS of the dissipated energy grows with increasing velocity with a local peak at the resonance velocity which corresponds to the maximum rail response. The lower the ballast/subgrade stiffness, the higher the overall level of RMS of dissipated energy. This conclusion is in line with that of a random support stiffness profile investigated in [23], where similar RMS behavior is predicted for different realizations of ballast stiffness from the same dataset. With respect to MDD of dissipated energy, the general trend is similar to that of RMS, namely lower ballast/subgrade stiffness is related to higher MDD. However, at higher velocities, the effect of the standard deviation of ballast stiffness on the MDD trend is not unique. Generally, however, for larger standard deviations of the stiffness and

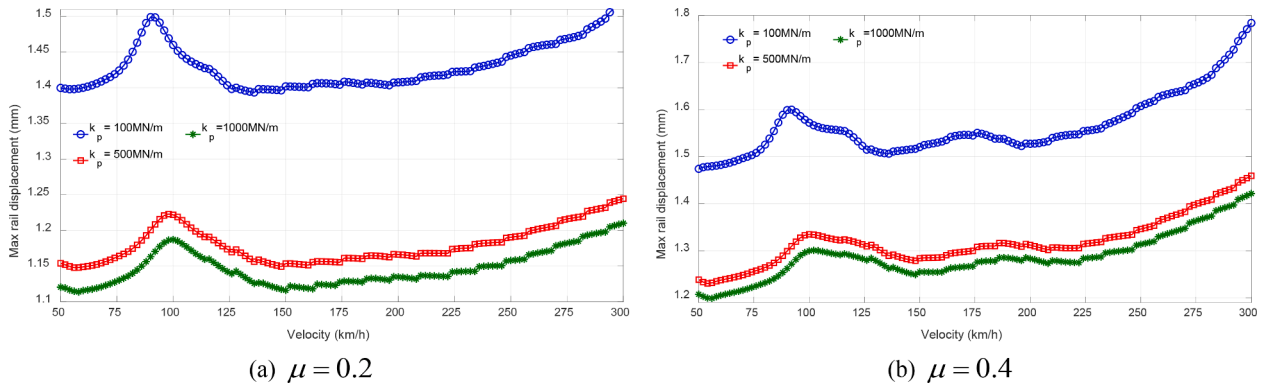


Fig. 12. Rail maximum displacement versus velocity ($\lambda = 4l_s$), different railpad stiffness.

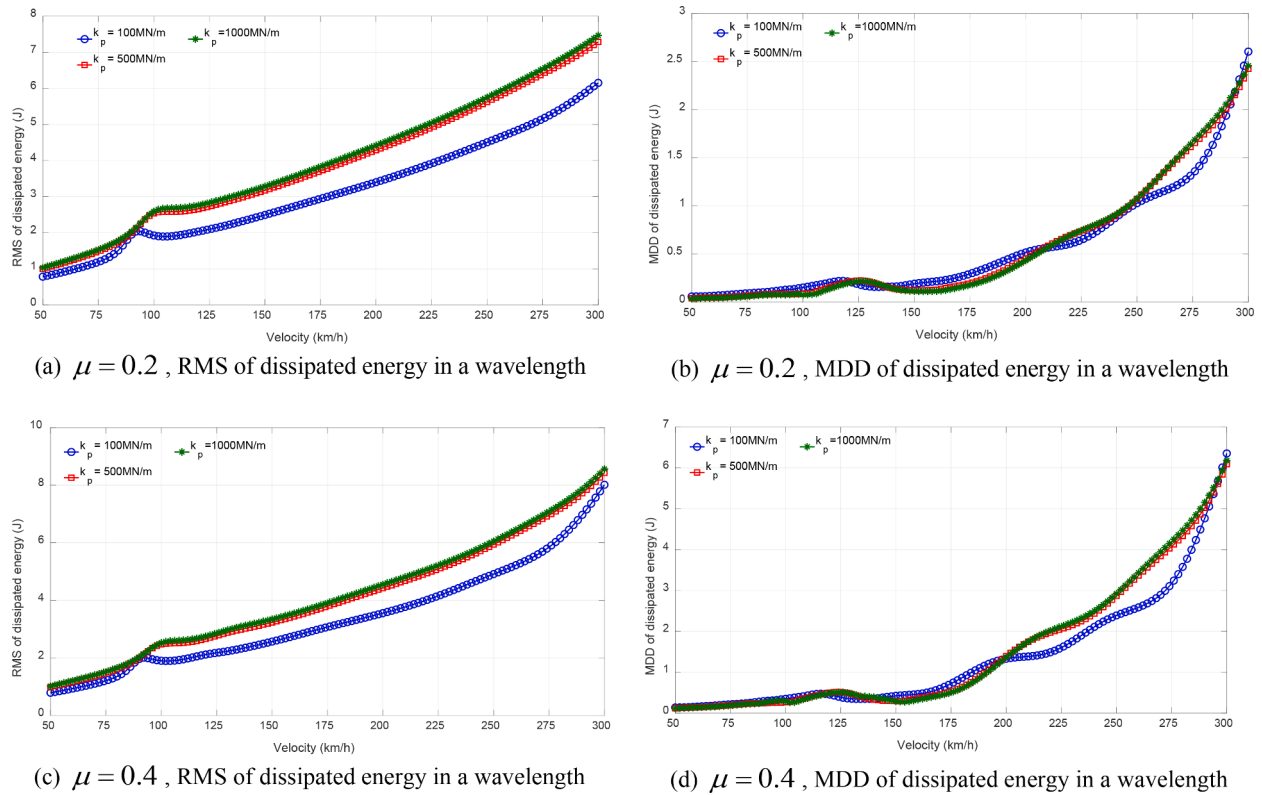


Fig. 13. RMS and MDD of dissipated energy ($\lambda = 4l_s$), different railpad stiffness.

especially in combination with higher train speeds, higher levels of dissipated energy in both representations RMS and MDD exist, indicating a higher expected rate of track degradation.

From the last two paragraphs, it can be concluded that in particular short-wave variation of rail support stiffness on soft subgrades contributes to track degradation and should therefore be avoided or mitigated in practice.

4.3. Influence of railpad stiffness

The influence of railpad stiffness is analyzed in this subsection. Three values of railpad stiffness (100 MN/m, 500 MN/m and 1000 MN/m) are chosen to demonstrate its effects. Other system parameters are selected to be the nominal value shown in Table 1.

Fig. 12 shows that a smaller railpad stiffness leads to a slightly lower resonance velocity. Since the ballast/subgrade stiffness dominates the rail support stiffness, the influence is less strong as that from the ballast/

subgrade stiffness. When the standard deviation of the ballast/subgrade stiffness increases, the rail displacement grows, while the trend with the velocity remains unaltered.

The dissipated energy in the ballast/subgrade increases with higher train velocity for both RMS and MDD (Fig. 13). However, as a rule of thumb it can be concluded that lower pad stiffnesses are favorable with respect to degradation, regardless of the value of the standard deviation of the ballast/subgrade stiffness.

5. Conclusions

A frequency-domain model, able to deal with parametric excitation due to both the discrete sleeper spacing and arbitrary large-scale spatial variation in track properties is used to study the effect of specific, harmonically varying support stiffness profiles on the long-term railway track behavior. The sensitivity to degradation is assessed by quantifying the energy dissipation in the substructure over one period of varying

support stiffness. The following conclusions can be drawn:

- (i) The inclusion of a harmonically varying ballast/subgrade stiffness introduces a new spatial period equaling the wavelength of the varying stiffness. As a result, extra resonance velocities corresponding to the spatial period-passing frequency of this new period are introduced which may significantly change the system response, but only for specific parameter combinations. On the other hand, inclusion of harmonically varying ballast/subgrade stiffness results in reduction of the response for major resonance speeds.
- (ii) The work clearly demonstrates the role of short wavelengths of varying ballast/subgrade stiffness as local degradation initiators, especially with increasing train speeds: these wavelengths lead to increasing energy dissipation in the substructure and work performed by the moving axle load. The same is valid for larger standard deviation of the ballast/subgrade stiffness magnitude. The energetic quantities vanish for wavelengths of approximately 16 times the sleeper span, for the case of one single moving axle, which is a length of approximately 10 m.
- (iii) When the mean value of the ballast/subgrade stiffness increases, the RMS and MDD of energy dissipation in the substructure decrease correspondingly, reaffirming that tracks on soft soils are in particular prone to degradation. Larger standard deviations of the support stiffness lead to higher energy dissipation.
- (iv) High railpad stiffness values result in higher energy dissipation; from this viewpoint stiff pads should be avoided in track design since they slightly increase the energy dissipation in the substructure and thus the track deterioration.
- (v) As a rule of thumb and with minor exceptions, an increasing train velocity amplifies the trends discussed under (iii-iv).

CRedit authorship contribution statement

Tao Lu: Methodology, Software, Investigation, Writing – original draft. **Rong Chen:** Data curation, Resources. **Ping Wang:** Data curation, Resources. **Junwei Wu:** Visualization, Validation. **Michael Steenbergen:** Conceptualization, Methodology, Writing – review & editing.

Declaration of Competing Interest

The authors declare that they have no known competing financial interests or personal relationships that could have appeared to influence the work reported in this paper.

Data availability

No data was used for the research described in the article.

Acknowledgements

This work is supported by the National Natural Science Foundation of China (NSFC) under grant No. 52108420. It is at the same time a further elaboration of a research project on long-term railway track performance carried out by Delft University of Technology and financed by ProRail. The work is also supported by the Natural Science Foundation of Sichuan (grant No. 2022NSFSC1908) and the Shanghai Key Laboratory of Rail Infrastructure Durability and System Safety (No. R202103).

References

- [1] Dahlberg T. Some railroad settlement models—A critical review. *Proc Inst Mech Eng, Part F: J Rail Rapid Transit.* 2001;215:289-300.
- [2] Dahlberg T. Railway track settlements—a literature review. Report for the EU project SUPERTRACK. 2004;463.
- [3] Frohling RD. Deterioration of railway track due to dynamic vehicle loading and spatially varying track stiffness. University of Pretoria; 2009.
- [4] Abadi T, Le Pen L, Zervos A, Powrie W. A review and evaluation of ballast settlement models using results from the Southampton Railway Testing Facility (SRTF). *Procedia Eng* 2016;143:999-1006.
- [5] Soleimanmeigouni I, Ahmadi A, Kumar U. Track geometry degradation and maintenance modelling: A review. *Proc Inst Mech Eng, Part F: J Rail Rapid Transit.* 2018;232:73-102.
- [6] Goodarzi S, Kashani HF, Oke J, Ho CL. Data-driven methods to predict track degradation: A case study. *Constr Build Mater* 2022;344:128166.
- [7] Khajehi H, Ahmadi A, Soleimanmeigouni I, Haddadzade M, Nissen A, Latif Jebelli MJ. Prediction of track geometry degradation using artificial neural network: a case study. *Int J Rail Transport* 2022;10:24-43.
- [8] Le Pen L, Milne D, Thompson D, Powrie W. Evaluating railway track support stiffness from trackside measurements in the absence of wheel load data. *Can Geotech J* 2016;53:1156-66.
- [9] Nielsen JC, Berggren EG, Hammar A, Jansson F, Bolmsvik R. Degradation of railway track geometry—Correlation between track stiffness gradient and differential settlement. *Proc Inst Mech Eng, Part F: J Rail Rapid Transit.* 2020;234:108-19.
- [10] Frýba L, Nakagiri S, Yoshikawa N. Stochastic finite elements for a beam on a random foundation with uncertain damping under a moving force. *J Sound Vib* 1993;163:31-45.
- [11] Náprstek J, Frýba L. Stochastic modelling of track and its substructure. *Veh Syst Dyn* 1995;24:297-310.
- [12] Oscarsson J. Dynamic train-track interaction: Variability attributable to scatter in the track properties. *Veh Syst Dyn* 2002;37:59-79.
- [13] Oscarsson J. Simulation of train-track interaction with stochastic track properties. *Veh Syst Dyn* 2002;37:449-69.
- [14] Andersen L, Nielsen SR. Vibrations of a track caused by variation of the foundation stiffness. *Probab Eng Mech* 2003;18:171-84.
- [15] Younesian D, Kargamovin MH. Response of the beams on random Pasternak foundations subjected to harmonic moving loads. *J Mech Sci Technol* 2009;23:3013-23.
- [16] Li M, Berggren E. A study of the effect of global track stiffness and its variations on track performance: simulation and measurement. *Proc Inst Mech Eng, Part F: J Rail Rapid Transit.* 2010;224:375-82.
- [17] Paixão A, Fortunato E, Calçada R. The effect of differential settlements on the dynamic response of the train-track system: A numerical study. *Eng Struct* 2015;88:216-24.
- [18] Germonpré M, Nielsen J, Degrande G, Lombaert G. Contributions of longitudinal track unevenness and track stiffness variation to railway induced vibration. *J Sound Vib* 2018;437:292-307.
- [19] Nielsen JC, Li X. Railway track geometry degradation due to differential settlement of ballast/subgrade—Numerical prediction by an iterative procedure. *J Sound Vib* 2018;412:441-56.
- [20] Wang H, Markine V. Modelling of the long-term behaviour of transition zones: Prediction of track settlement. *Eng Struct* 2018;156:294-304.
- [21] Grossoni I, Andrade AR, Bezin Y, Neves S. The role of track stiffness and its spatial variability on long-term track quality deterioration. *Proc Inst Mech Eng, Part F: J Rail Rapid Transit.* 2019;233:16-32.
- [22] Sadri M, Lu T, Steenbergen M. Railway track degradation: The contribution of a spatially variant support stiffness-Local variation. *J Sound Vib* 2019;455:203-20.
- [23] Sadri M, Lu T, Steenbergen M. Railway track degradation: The contribution of a spatially variant support stiffness-Global variation. *J Sound Vib* 2020;464:114992.
- [24] Milne D, Harkness J, Le Pen L, Powrie W. The influence of variation in track level and support system stiffness over longer lengths of track for track performance and vehicle track interaction. *Veh Syst Dyn* 2021;59:245-68.
- [25] Phadke H, Jaiswal O. Dynamic analysis of railway track on variable foundation under harmonic moving load. *Proc Inst Mech Eng, Part F: J Rail Rapid Transit.* 2022;236:302-16.
- [26] Tran L-H, Hoang T, Foret G, Duhamel D. Calculation of the dynamic responses of a railway track on a non-uniform foundation. *J Vib Control* 2023;29(15-16):3544-53.
- [27] Paixão A, Fortunato E, Calçada R. Transition zones to railway bridges: track measurements and numerical modelling. *Eng Struct* 2014;80:435-43.
- [28] Shan Y, Zhou S, Wang B, Ho CL. Differential settlement prediction of ballasted tracks in bridge-embankment transition zones. *J Geotech Geoenviron Eng* 2020;146:04020075.
- [29] Grossoni I, Powrie W, Zervos A, Bezin Y, Le Pen L. Modelling railway ballasted track settlement in vehicle-track interaction analysis. *Transp Geotech* 2021;26:100433.
- [30] Charoenwong C, Connolly D, Woodward P, Galvín P, Costa PA. Analytical forecasting of long-term railway track settlement. *Comput Geotech* 2022;143:104601.
- [31] de Oliveira Barbosa JM, Färågåu AB, van Dalen KN, Steenbergen MJMM. Modelling ballast via a non-linear lattice to assess its compaction behaviour at railway transition zones. *J Sound Vib* 2022;530:116942.
- [32] Metrikine A, Vostrukhov A, Vrouwenvelder A. Drag experienced by a high-speed train due to excitation of ground vibrations. *Int J Solids Struct* 2001;38:8851-68.

- [33] Fărăgău AB, Mazilu T, Metrikine AV, Lu T, van Dalen KN. Transition radiation in an infinite one-dimensional structure interacting with a moving oscillator—the Green's function method. *J Sound Vib* 2021;492:115804.
- [34] Steenbergen MJMM. Physics of railroad degradation: The role of a varying dynamic stiffness and transition radiation processes. *Comput Struct* 2013;124:102–11.
- [35] Nasrollahi K, Nielsen JC, Aggestam E, Dijkstra J, Ekh M. Prediction of long-term differential track settlement in a transition zone using an iterative approach. *Eng Struct* 2023;283:115830.